Oxygen vacancy engineering of TaO_x-based resistive memories by Zr doping for improved variability and synaptic behavior

João Palhares, Yann Beilliard, F. Alibart, Everton Bonturim, Daniel de Florio, Fabio Fonseca, Dominique Drouin, Andre Ferlauto

PAPER • **OPEN ACCESS**

Oxygen vacancy engineering of TaO_x-based resistive memories by Zr doping for improved variability and synaptic behavior

To cite this article: João H Quintino Palhares *et al* 2021 *Nanotechnology* **32** 405202

OPEN ACCESS
IOP Publishing
Nanotechnology

Nanotechnology **32** (2021) 405202 (8pp)
https://doi.org/10.1088/1361-6528/ac0e67

Oxygen vacancy engineering of TaO_x-based resistive memories by Zr doping for improved variability and synaptic behavior

João H Quintino Palhares[1,2,*], Yann Beilliard[2,3,4], Fabien Alibart[2,3,5], Everton Bonturim[6], Daniel Z de Florio[1], Fabio C Fonseca[7], Dominique Drouin[2,3,4,*] and Andre S Ferlauto[1,*]

[1] CECS, Federal University of ABC, Santo André 09210-580, SP, Brazil
[2] Institut Interdisciplinaire d'Innovation Technologique (3IT), Université de Sherbrooke, Sherbrooke J1K 0A5, Canada
[3] Laboratoire Nanotechnologies Nanosystèmes (LN2)—CNRS UMI-3463—3IT, CNRS, Sherbrooke J1K 0A5, Canada
[4] Institut Quantique (IQ), Université de Sherbrooke, Sherbrooke J1K 2R1, Canada
[5] Institute of Electronics, Microelectronics and Nanotechnology (IEMN), Université de Lille, F-59650, Villeneuve d'Ascq, France
[6] Department of Chemistry, School of Engineering, Mackenzie Presbyterian University, 01302907, São Paulo, SP, Brazil
[7] Nuclear and Energy Research Institute, IPEN-CNEN, São Paulo, 05508-000, Brazil

E-mail: quij2205@usherbrooke.ca, andre.ferlauto@ufabc.edu.br and dominique.drouin@usherbrooke.ca

Received 21 April 2021
Accepted for publication 23 June 2021
Published 12 July 2021

Abstract

Resistive switching (RS) devices are promising forms of non-volatile memory. However, one of the biggest challenges for RS memory applications is the device-to-device (D2D) variability, which is related to the intrinsic stochastic formation and configuration of oxygen vacancy (V_O) conductive filaments (CFs). In order to reduce the D2D variability, control over the formation and configuration of oxygen vacancies is paramount. In this study, we report on the Zr doping of TaO_x-based RS devices prepared by pulsed-laser deposition as an efficient means of reducing the V_O formation energy and increasing the confinement of CFs, thus reducing D2D variability. Our findings were supported by XPS, spectroscopic ellipsometry and electronic transport analysis. Zr-doped films showed increased V_O concentration and more localized V_Os, due to the interaction with Zr. DC and pulse mode electrical characterization showed that the D2D variability was decreased by a factor of seven, the resistance window was doubled, and a more gradual and monotonic long-term potentiation/depression in pulse switching was achieved in forming-free Zr:TaO_x devices, thus displaying promising performance for artificial synapse applications.

Supplementary material for this article is available online

Keywords: TaO_x, oxygen vacancy engineering, memristor, variability, doping, resistive switching, synaptic behavior

(Some figures may appear in colour only in the online journal)

* Authors to whom any correspondence should be addressed.

1. Introduction

Resistive switching (RS) memories based on oxide thin films are a promising technology for next-generation high-density non-volatile memory applications and the hardware implementation of artificial neural networks [1–4], due to their impressive switching operation performance in terms of speed, endurance, scaling and multistate resistance modulation [5–8]. However, both cycle-to-cycle (C2C) and device-to-device (D2D) variability in the switching characteristics still hinders the widespread use of this technology, as these reduce the average performance and generate cost increases due to the need for complex overhead circuits [5, 9, 10]. RS is generated by the creation and dissolution of conductive channels within an oxide layer in a capacitor-like structure, as a result of the nanoionic movement of oxygen vacancies (V_O) under the application of high electric fields [11, 12]. An initial operation step called a forming process is typically required in order to generate sufficient V_Os to allow for the formation of conductive filaments (CFs). The stochastic nature of the forming and switching steps leads to slightly different CF configurations for each device, resulting in D2D and C2C variability [5, 10, 12–16]. Understanding and control of the formation, movement and arrangement of V_Os in RS devices is therefore paramount [13, 17, 18].

Various strategies have been explored for the creation of excess oxygen vacancies in a controlled manner, in order to mitigate forming-induced variability [19–21]. The most common and direct method of V_O generation is intrinsic doping, i.e. the use of low oxygen partial pressure during fabrication of the oxide layer, using methods such as reactive sputtering or pulsed-laser deposition (PLD). This approach has been particularly successful for tantalum oxide films [20–22]. Intrinsic doping has certain limitations, however, as it is difficult to control, relies on external parameters and is subject to instabilities in the processing conditions [17, 23–25]. A more reliable alternative is extrinsic doping, which consists of adding dopant atoms with a valence that is lower than the host metal cation; this leads to the formation of V_Os in order to maintain electroneutrality [12, 17, 26, 27]. Extrinsic doping also helps to reduce the randomness of V_O generation. Theoretical studies of Ta_2O_5 doped with Ti, Zr and Al have indeed shown that the formation of V_Os is favored near the dopant species [26]. In these cases, charged V_Os are compensated and attracted by p-type dopants, forming dopant-V_O complexes. These complexes trap V_Os, and can interconnect to form CFs. A reduction in variability has been experimentally observed for extrinsically doped TaO_x [28] and HfO_2 based [29, 30] devices. It has been claimed that implanted or embedded dopant elements (e.g. Gd, Al) in HfO_2 help to localize V_O formation and lead to more confined CFs, resulting in significantly lower device variability. This interaction between the dopant species and V_Os can change the switching dynamics and switching voltage operation [18], meaning that extrinsic doping can be leveraged to further optimize switching performance for specific applications, such as artificial synapses.

In this work, we report the fabrication of TaO_x-based memristors with reduced D2D variability and controllable pulse switching dynamics, thanks to doping of the active layer with Zr. For comparison purposes, Zr-doped (Zr:TaO_x) and pure TaO_x-based devices were prepared in an oxygen-poor atmosphere using PLD. Oxygen-poor conditions are used to suppress electroforming step and its effect on the active layer properties. The chemical compositions of both types of devices were investigated using x-ray photoelectron spectroscopy (XPS) analysis and spectroscopic ellipsometry (SE). RS investigations in DC and pulsed mode revealed that D2D variability was decreased by a factor of seven, the resistance window was doubled and more gradual and monotonic long-term potentiation and depression (LTP/LTD) in pulse switching was achieved in Zr:TaO_x devices. By analyzing the device current density–electric field (*J–E*) curves using a hopping transport model, we demonstrate that Zr:TaO_x devices have a higher V_O concentration and a lower variability of this concentration between different devices.

2. Methods

Devices were fabricated on silicon substrates covered with 200 nm of SiO_2 (figure 1(a)). Sputtering was used to deposit tungsten (W) on the bottom (BE) and top electrodes. The latter were patterned to give 80 μm round pads, using UV photolithography and lift-off. TaO_x and Zr:TaO_x layers were deposited at room temperature via PLD (with a TSST system) using a Ta_2O_5 target and a Ta_2O_5:20 mol% ZrO_2 target, respectively, at a target−substrate distance of 45 mm, with a laser fluence of 3 J cm^{-2} and a repetition rate of 10 Hz under an oxygen flow of 2 sccm. Layer thickness was estimated to be 10 nm by using the growth rate as determined by SE measurements. Based on previous studies [22], we used an O_2 partial pressure of 2×10^{-2} mbar to induce the formation of slightly sub-stoichiometric active layers. The generation of V_Os by extrinsic and intrinsic doping was investigated using XPS (KRATOS Axis UltraDLD), SE (JA Woollam, model M-2000) and *J–E* conduction transport analysis of the devices. The electrical properties of the RS devices under DC and pulsed conditions were carried out with a Keithley S4200 semiconductor parameter analyzer and a Keithley 4225-PMU module. For all measurements, the BE was grounded and the signals were applied to the top electrodes.

3. Results and discussions

The thin films were analyzed using XPS and SE. The ratios (O/M) between oxygen and the sum of the metal atoms (M = [Ta] for TaO_x and M = [Ta] + [Zr] for Zr:TaO_x) was determined by quantification of the Ta 4f, Zr 3d and O 1s peaks shown in figures 1(b)−(d)). Due to the low pO_2 during deposition, TaO_x and Zr:TaO_x films had O/M ratios of 2.45 and 2.25, respectively. This is lower than the value of O/M = 2.5 corresponding to the oxygen concentration of the stoichiometric tantalum pentoxide (Ta_2O_5), thus indicating the presence of V_O [20, 21]. This effect was also confirmed

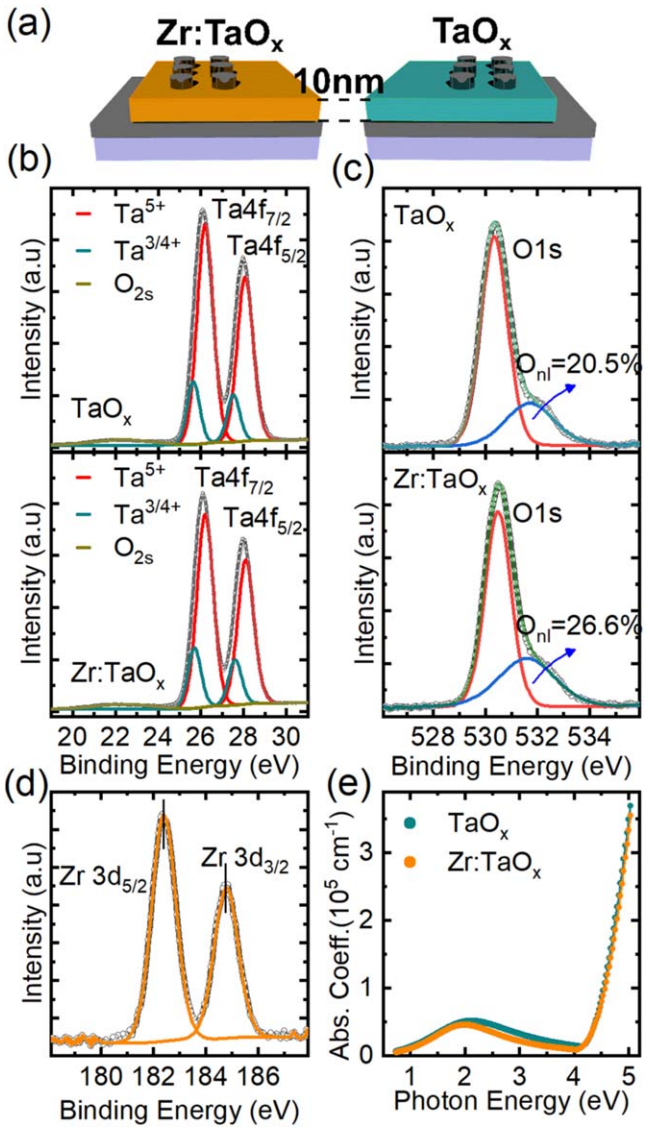

Figure 1. (a) Schematic of W/Zr:TaO$_x$/W and W/TaO$_x$/W RS devices and active layer characterization results: (b) XPS analysis of Ta 4f, (c) O 1s and (d) Zr 3d peaks for the Zr:TaO$_x$ and TaO$_x$ samples. (e) Absorption spectra of TaO$_x$ and Zr:TaO$_x$ obtained via SE.

by the change in the XPS Ta 4f peak, which suggests the presence of Ta cations in lower valence states (Ta^{4+} and Ta^{3+}) (figure 1(b)). The energy positions of the chemical components Ta^{5+}, Ta$^{3/4+}$ and O 2s were 26.3, 25.7 and 22 eV, respectively. For the Ta 4f components, the area ratio was fixed at 0.75 and the spin–orbit splitting at 1.9 eV [20, 31]. The presence of Ta in a lower oxidation state is expected to result from the partial reduction of tantalum oxide (intrinsic doping), as given by the following reaction in Kröger–Vink notation [32]

$$2\mathrm{Ta}_{\mathrm{Ta}}^{x} + \mathrm{O}_{\mathrm{O}}^{x} \rightarrow 2\mathrm{Ta}_{\mathrm{Ta}}^{\prime} + \mathrm{V}_{\mathrm{O}}^{\cdot\cdot} + \frac{1}{2}\mathrm{O}_{2(g)}. \quad (1)$$

As expected, the Zr-doped films are more sub-stoichiometric, since the presence of Zr^{4+} cations induces V$_O$ formation according to the reaction

$$2\mathrm{ZrO}_2 \xrightarrow{\mathrm{Ta_2O_5}} 2\mathrm{Zr}_{\mathrm{Ta}}^{\prime} + \mathrm{V}_{\mathrm{O}}^{\cdot\cdot} + 4\mathrm{O}_{\mathrm{O}}^{x}. \quad (2)$$

Furthermore, as shown in figure 1(c), the O 1s peaks have an asymmetric line shape that can be deconvoluted into two components centered at 531.3 and 530.0 eV; these can be assigned to non-lattice (O$_{nl}$) and lattice oxygen, respectively. The non-lattice oxygen peak can be associated with the presence of V$_O$ [33, 34]. The fact that Zr:TaO$_x$ films contain a larger percentage of non-lattice oxygen (26%) compared to TaO$_x$ films (20%) suggests that Zr^{4+} substitution indeed promotes V$_O$ formation. This is in agreement with results reported by Park *et al* [35] for KNBO films doped with Cu^{2+}, and by Kim *et al* [36] for Si-doped tantalum oxide-based memristors. The XPS spectrum for the Zr 3d peak was deconvoluted into Zr 3d$_{3/2}$ and Zr 3d$_{5/2}$, centered at 182.4 and 184.7 eV respectively [37–39], corresponding to Zr^{4+} states (figure 1(d)). The nominal relative concentration of Zr with respect to the concentration of Ta atoms [Zr]/[Ta] was determined as 8%.

Figure 1(e) shows the optical absorption spectra obtained by fitting the ellipsometry data using a Tauc-Lorentz analytical function, which is widely used to describe the optical properties of amorphous and polycrystalline semiconductors and dielectric films [40, 41]. In this function, the imaginary part of the dielectric function is described by a Tauc expression for photon energies above the gap, and is forced to zero below the band gap. The overall interband transition in the higher range of photon energies analyzed here is described by a Lorentz oscillator. Although this function can be used to describe pure stoichiometric dielectric Ta$_2$O$_5$ films, absorption in the sub-gap region is observed for sub-stoichiometric films. This feature can be modeled using a broad Lorentz function. Sub-gap absorption has been observed previously in sub-stoichiometric TaO$_x$ films [42], and was associated with the presence of V$_O$s [43–45]. From figure 1(e), it can be seen that the optical responses of both TaO$_x$ and Zr:TaO$_x$ exhibit considerable sub-gap absorption, thus confirming the XPS results. It is interesting to note that the optical absorption intensity is similar for both samples, even though the Zr-doped films have a higher V$_O$ concentration. One possible explanation for this is that the dopant-V$_O$ interaction may suppress the optical activity of the V$_O$ due to changes in the charge [18, 44].

To gain insight into the effects of Zr doping on the characteristics and variability of RS, current- and DC voltage-controlled sweeps were used for SET and RESET operations, respectively. For each device, in the SET and RESET operation, the current compliance and the maximum operation voltage values, respectively, were defined to maximize the device resistance window while avoiding irreversible damage. These values slightly vary among devices due to an intrinsic variation in the threshold voltage and maximum resistance window of each device. Figure 2 shows RS characterizations of W/TaO$_x$/W (figure 2(a)) and W/Zr:TaO$_x$/W (figure 2(b)) devices. Up to five full RS cycles were performed on each device, and the resistance state was measured at 0.2 V. For

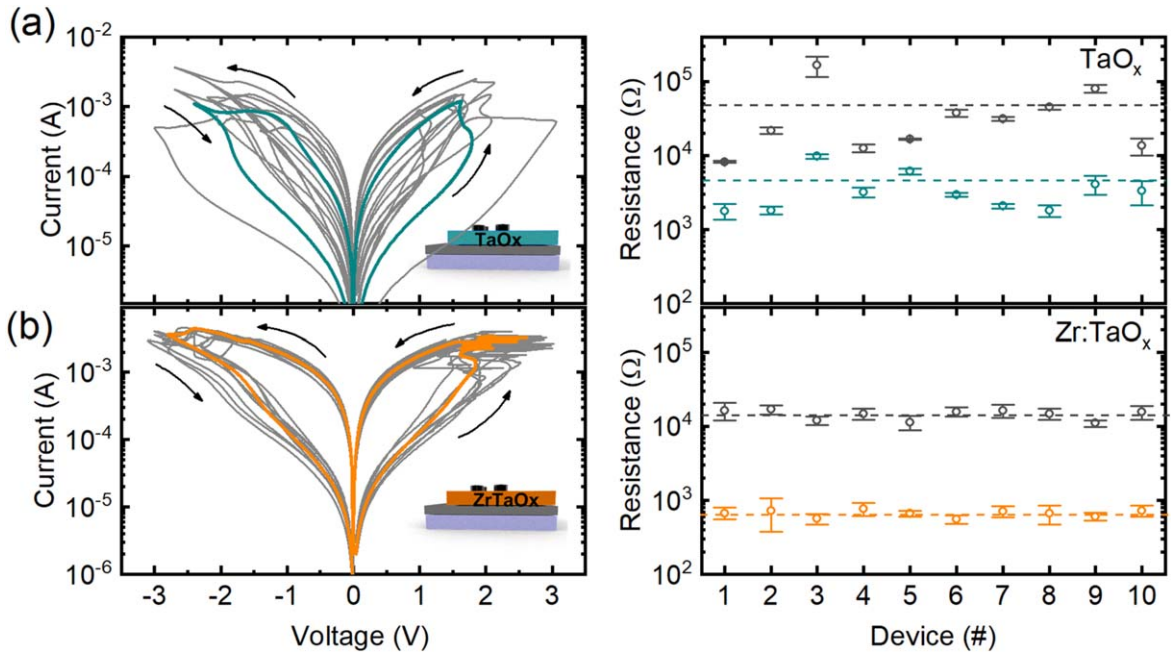

Figure 2. Current–voltage (I–V) characteristics for the 10 devices tested, with a statistical analysis of the resistance states per device: (a) W/TaO_x/W RS devices and (b) W/Zr:TaO_x/W RS devices. To improve visibility, the switching curve for one random device is shown in color. The resistance was measured at 0.2 V. The resistance values for the Zr:TaO_x devices exhibit improved D2D variability.

Table 1. Comparison of key parameters of Zr:TaO_x- and TaO_x-based memristors

	Zr:TaO_x		TaO_x	
	$\mu \pm \sigma$	CV (%)	$\mu \pm \sigma$	CV (%)
LRS/HRS	21.8 ± 3.3	15.1	12.5 ± 7.6	60.8
R_{LRS} (kΩ) @0.2 V	0.70 ± 0.07	10.0	3.7 ± 2.7	73.0
R_{HRS} (kΩ) @0.2 V	14.5 ± 2.2	15.2	46.5 ± 49.6	106.7
J(A cm^{-2}) @0.2 V – LRS	6.0 ± 0.7	11.6	1.4 ± 0.7	50.0
J(A cm^{-2}) @0.2 V – HRS	0.30 ± 0.05	16.7	0.20 ± 0.10	50.0
V_{SET} (V)	2.3 ± 0.4	17.4	1.7 ± 0.5	29.4
V_{RESET} (V)	2.3 ± 0.5	21.7	2.0 ± 0.6	30.0
a (nm) – HRS	0.6 ± 0.1	16.7	0.7 ± 0.2	29.0
a (nm) – Pristine	1.0 ± 0.2	20.0	1.6 ± 0.7	43.8
$[n_{Vo}]$ (10^{21}/cm^{-3}) – HRS	6.6 ± 3.4	51.5	5.5 ± 4.4	80.0
$[n_{Vo}]$ (10^{21}/cm^{-3}) – Pristine	1.5 ± 1.4	93.3	1.1 ± 1.8	163.6

more RS cycles and performance information see supplementary material (available online at stacks.iop.org/NANO/32/405202/mmedia). In each RS plot, ten switching curves (the last RS cycle of each device) are given, corresponding to ten different devices with the same stack structure. The coefficient of variation (CV), defined as the standard deviation (σ) divided by the average value (μ) of a given device parameter, is used to account for the variability and dispersion. Table 1 summarizes the statistical data for main RS parameters. In the pristine state, most devices had resistance values ranging between the subsequent high resistance states (HRSs) and low resistance states (LRSs), and hence a forming process was not required. Few devices had initial resistance values higher than the HRS values, and these were switched with a voltage that was lower than in the subsequent SET and RESET operations. For both the Zr:TaO_x and TaO_x devices, the forming-free behavior was due to the high vacancy concentrations resulting from both intrinsic and extrinsic Zr^{4+} doping [20, 21]. The devices showed bipolar switching, with the SET operation occurring with a positive bias (V_{SET}) and the RESET operation with a negative bias (V_{RESET}) for all devices. The average values of V_{RESET}, V_{SET} were slightly increased for Zr:TaO_x devices (up to ∼2.3 V as compared with ∼2 V for TaO_x), an effect that can be ascribed to the dopant-V_O interaction that may lead to defect clustering and consequent change in defect mobility. In addition, the current density values (@0.2 V) were slightly higher for the Zr:TaO_x devices, which can be explained by the increased V_O concentration. C2C variability in LRS and HRS resistance was similar for both the Zr:TaO_x and TaO_x devices, with average values for the CV of around 18% and 14%, respectively (see the curves in the supporting information). On the other hand,

significant contrast was observed in the D2D variability, and especially in the resistance values in both the LRS and HRS states, in which the CV for the Zr:TaO_x device in the LRS was reduced from 68% to 9% and in the HRS from 110% to 15% compared to TaO_x (see table 1). Another important feature observed for the Zr:TaO_x devices was an increase in the average resistance window, from 12.5 for the TaO_x-based devices to 21.8 for the Zr-doped ones. A similar contrast was previously noted in a comparison of sub-stoichiometric to purely stoichiometric TaO_x devices [20], and was attributed to CF confinement and an increase in carrier concentration, which results in higher current densities. This localized Joule effect gives rise to greater filament dissolution and thus a larger resistance window [20]. These results indicate that Zr doping helps to improve RS performance by lowering D2D variability.

To further evaluate the effects of doping on the transport mechanisms, we conducted a carrier transport analysis by applying a hopping model that has been used previously in studies of tantalum oxide-based devices [46–48]. The *J–E* curves for the devices in both the pristine state and the HRS were fitted using the following expression [47, 49, 50]

$$J = qanv \exp\left(\frac{qaE}{k_B T} - \frac{\varnothing_t}{k_B T}\right), \tag{3}$$

where a denotes the average distance between trap sites, $\varnothing_t$ is the trap energy, k_B is the Boltzmann constant, q is the electronic charge, n is the carrier concentration and ν is the attempt-to-escape frequency. As can be seen from figures 3(a)–(d), the *I–V* characteristics are well described by the hopping model (the fitted curves and parameters extracted for all devices are provided in the supplementary material). The values obtained for the average distance between traps for pristine Zr:TaO_x- and TaO_x-based devices were 1.0 ± 0.2 and 1.6 ± 0.7 nm, respectively (see table 1). The HRS trap distances were 0.6 ± 0.1 and 0.7 ± 0.2 nm for Zr:TaO_x and TaO_x devices, respectively. The trap concentration for each type of device can be estimated by calculating [51, 52]

$$[n_{\mathrm{Vo}}] = a^{-3}. \tag{4}$$

Pristine Zr:TaO_x devices had a higher concentration of traps, with a value of $(1.5 \pm 1.4) \times 10^{21}$ cm^{-3} compared with $(1.1 \pm 1.8) \times 10^{21}$ cm^{-3} for TaO_x devices. The same trend was observed for the HRS states: the Zr:TaO_x-based device has a trap concentration of traps $(6.6 \pm 3.4) \times 10^{21}$ cm^{-3} as compared to $(3.6 \pm 1.1) \times 10^{21}$ cm^{-3} for TaO_x.

The transport mechanism in TaO_x films depends critically on the V_O concentration. TaO_x exhibits Fermi glass behavior, in which V_O complexes are trap sites and transport occurs via electron hopping [53, 54]. An increase in V_O concentration gives rise to a percolation process, and once the fraction of hopping sites exceeds a certain threshold, they form a continuous conductive path. The results in figure 3 indicate that the distances between traps for both Zr:TaO_x and TaO_x devices are in good agreement with reference values [44, 48, 54, 55]. The shorter distance in the Zr:TaO_x-based devices explains the increased current density (@0.2 V). It is also important to emphasize that the variability of the devices

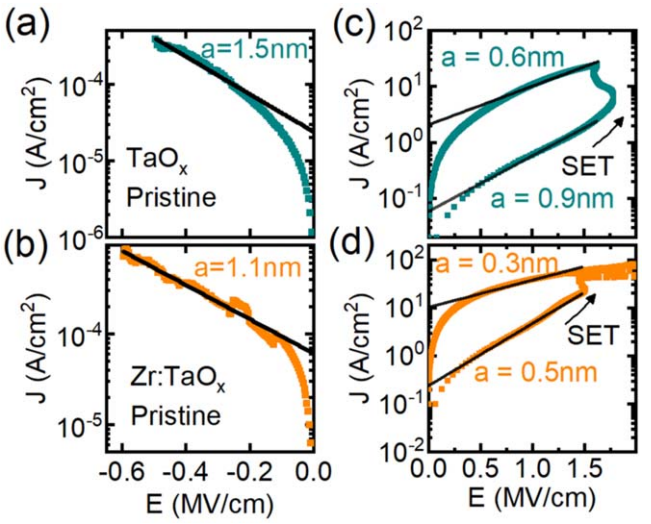

Figure 3. Experimental *J–E* plot and hopping model with fitted lines and extracted hopping distances for pristine (a) TaO_x and (b) Zr:TaO_x devices, and subsequent LRSs and HRSs for (c) TaO_x and (d) Zr:TaO_x. Zr:TaO_x-based devices have a lower distance between traps in all resistance states.

is directly correlated with the variability in the distance between V_Os or V_O concentration, indicating that extrinsic doping is a more controllable way of changing the V_O configuration.

In order to assess the synaptic-like behavior of the devices, the switching dynamics were evaluated using pulsed measurements. We investigated comparative potentiation and depression characteristics using same time interval for LTP and LTD. As shown in figure 4(a), a sequence of 200 pulses for each LTD and LTP process was performed using time intervals of 200 μs and 600 ns, respectively. The LTD voltage amplitudes used were 2.4 V and 3.2 V, and LTP voltages were 2.1 V and 3.0 V for the TaO_x and Zr:TaO_x devices, respectively. The values of the applied voltage for the TaO_x and Zr:TaO_x devices were different because the voltage for RS operation is higher for the latter, as previously discussed. However, even at a higher voltage amplitude, it was observed that Zr:TaO_x had more gradual potentiation and depression dynamics in its operation at a similar LRS/HRS ratio, as shown in the normalized pulse switching curves in figures 4(b), (c). CV for both maximum and minimum conductance states are given for nine full LTD/LTP cycles. A non-monotonic increase in conductance can be seen in the first few potentiation pulses in the TaO_x-based device, and it has been claimed that this is related to a competition between thermal- and field-driven effects on the movement of V_Os and the consequent CF stability [56]. This feature is detrimental for synaptic applications where weight update dynamics should be monotonic. The LTP curve for Zr:TaO_x devices does not exhibit this problem however. This improvement can be attributed to the additional energy needed to overcome the attractive interaction between V_Os and Zr cations. Although extrinsic doping generates a higher vacancy concentration, the trapping of V_Os by dopant-Vo complexes also leads to a reduction in the overall V_O kinetics. This tunability of the

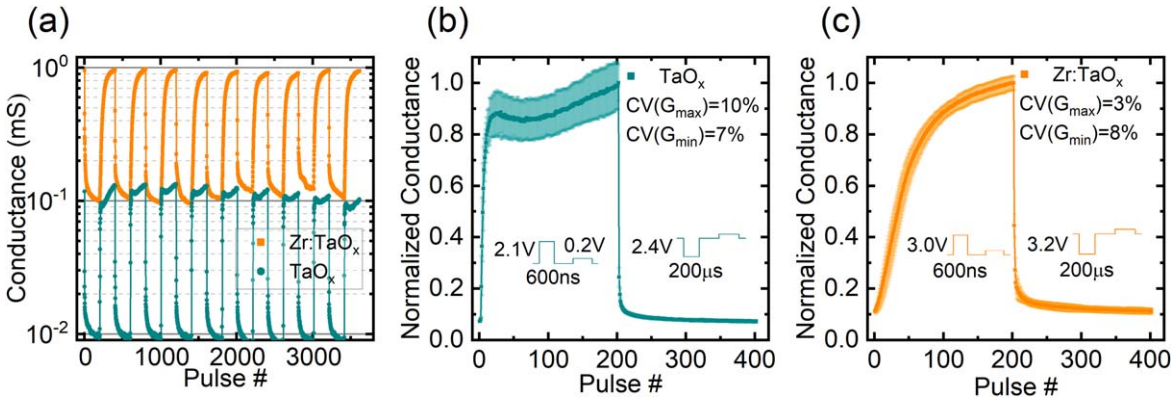

Figure 4. (a) Conductance values as a function of the number of pulses, plotted on a semi-log scale. Nine repeated pulsed-based LTD and LTP operations are shown, and synaptic weight emulation is demonstrated for the W/TaO$_x$/W (green) and W/Zr:TaO$_x$/W (orange) RS devices. (b), (c) Average conductance and standard deviation as a function of the number of pulses for nine full LTD/LTP cycles of TaO$_x$ and Zr:TaO$_x$ devices. The latter exhibit a more gradual, reproducible, and monotonic variation of the conductance. CV of maximum (G$_{max}$) and minimum (G$_{min}$) conductance states are shown for both devices.

switching dynamics through extrinsic doping can be generalized to other p-type dopants, as previously mentioned by Lübben *et al* [18]

Low C2C and D2D variability has been associated with a more reproducible formation and homogenous distribution of CFs [14, 57]. In this work, the decrease in D2D variability cannot be attributed solely to the higher concentration of V_O, but is also related to the interaction between V_Os and dopant species, which promotes V_O localization around the dopant cations. This interaction has been well described for several doped oxides, in both experimental and theoretical simulation studies [26–28]. This localization may provide a guiding path for the formation of CFs, resulting in a less random distribution of CFs along the active layer. Moreover, simulation has shown that the presence of dopants reduces the V_O formation energy [26, 27]. It is interesting to note that Ambrogio *et al* [58] have demonstrated that device variability is associated with fluctuations in V_O energy barrier for hopping conduction. It can be argued that the presence of the dopant reduces this fluctuation, thus pinning the V_O energy to a fixed value and reducing the variability. The V_O-dopant interaction is also reflected in the slower V_O kinetics and the consequent change in the pulsed switching dynamics.

In this study, we have demonstrated that doping can be used to tune the V_O content and consequently the defect trap density and CF configuration in tantalum oxide-based memristor devices. It was shown that Zr doping (extrinsic doping) and control over the partial pressure of oxygen during PLD (intrinsic doping) can promote V_O formation and lead to forming-free devices. In addition, extrinsic doping proved to be better in terms of controlling the V_O configuration and content. The unique effect of Zr doping is that it localizes V_Os and consequently reduces the D2D variability. It was also used to tune the pulse switching dynamics for the devices. This enhancement in device parameters in terms of switching variability and dynamics reinforces the importance of exploring vacancy engineering for the tuning of memristor behavior for high-density memory applications and memristor-based artificial synapses.

See the supplementary material for additional information on target preparation, C2C variability, device performance (endurance), hopping model fitted curves, retention measurements and thin film topography using an atomic force microscope.

Acknowledgments

This work was supported by Natural Sciences and Engineering Research Council of Canada (NSERC). Financial support of CNPq (INCT Carbon Nanomaterials), CNEN, Center for Innovation on New Energies-CINE SHELL (ANP) / FAPESP 2017/11937-4, FAPESP (14/50279-4) and Coordenação de Aperfeiçoamento de Pessoal de Nível Superior-Brasil (CAPES)-Finance Code 001, is acknowledged. This research was undertaken thanks in part to funding from the Canada First Research Excellence Fund. We would like to acknowledge Abdelouadoud El Mesoudy and Wellington de Oliveira Avelino from 3IT for their help and insightful discussions regarding device electrical characterizations, and Sonia Blais from Plateforme de Recherche et d'Analyse des Matériaux (PRAM) at the Université de Sherbrooke for her support with XPS measurements. We also acknowledge LCPNano at the Federal University of Minas Gerais (UFMG) for providing access to the clean room facility and for ellipsometry measurements.

Data availability statement

The data that support the findings of this study are available upon reasonable request from the authors.

ORCID iDs

João H Quintino Palhares https://orcid.org/0000-0002-2820-1627
Yann Beilliard https://orcid.org/0000-0003-0311-8840

Everton Bonturim https://orcid.org/0000-0001-5302-9091
Daniel Z de Florio https://orcid.org/0000-0002-7291-1917
Fabio C Fonseca https://orcid.org/0000-0003-0708-2021
Andre S Ferlauto https://orcid.org/0000-0003-3056-7289

References

[1] Waser R, Dittmann R, Staikov C and Szot K 2009 Redox-based resistive switching memories nanoionic mechanisms, prospects, and challenges *Adv. Mater.* **21** 2632–63
[2] Strukov D B, Snider G S, Stewart D R and Williams R S 2008 The missing memristor found *Nature* **453** 80–3
[3] Wang J and Zhuge F 2019 Memristive synapses for brain-inspired computing *Adv. Mater. Technol.* **4** 1–20
[4] Amirsoleimani A, Alibart F, Yon V, Xu J, Pazhouhandeh M R, Ecoffey S, Beilliard Y, Genov R and Drouin D 2020 In-memory vector-matrix multiplication in monolithic complementary metal-oxide-semiconductor-memristor integrated circuits: design choices, challenges, and perspectives *Adv. Intell. Syst.* **2** 2000115
[5] Yang J J, Strukov D B and Stewart D R 2013 Memristive devices for computing *Nat. Nanotechnol.* **8** 13–24
[6] Lee M *et al* 2011 A fast, high-endurance and scalable non-volatile memory device made from asymmetric Ta_2O_{5-x}/TaO_{2-x} bilayer structures *Nat. Mater.* **10** 625–30
[7] Yang J J, Zhang M X, Strachan J P, Miao F, Pickett M D, Kelley R D, Medeiros-Ribeiro G and Williams R S 2010 High switching endurance in TaO_x memristive devices *Appl. Phys. Lett.* **97** 6–9
[8] Torrezan A C, Strachan J P, Medeiros-Ribeiro G and Williams R S 2011 Sub-nanosecond switching of a tantalum oxide memristor *Nanotechnology* **22** 485203
[9] Kim K M, Yang J J, Strachan J P, Grafals E M, Ge N, Melendez N D, Li Z and Williams R S 2016 Voltage divider effect for the improvement of variability and endurance of TaO_x memristor *Sci Rep.* **6** 1–6
[10] Guan X, Yu S and Wong H S P 2012 On the switching parameter variation of metal-oxide RRAM: I. Physical modeling and simulation methodology *IEEE Trans. Electron Devices* **59** 1172–82
[11] Celano U, Goux L, Degraeve R, Fantini A, Richard O, Bender H, Jurczak M and Vandervorst W 2015 Imaging the three-dimensional conductive channel in filamentary-based oxide resistive switching memory *Nano Lett.* **15** 7970–5
[12] Lee J and Lu W D 2018 On-demand reconfiguration of nanomaterials: when electronics meets ionics *Adv. Mater.* **30** 1–33
[13] Baeumer C *et al* 2017 Subfilamentary networks cause cycle-to-cycle variability in memristive devices *ACS Nano* **11** 6921–9
[14] Fantini A, Goux L, Degraeve R, Wouters D J, Raghavan N, Kar G, Belmonte A, Chen Y Y, Govoreanu B and Jurczak M 2013 Intrinsic switching variability in HfO_2 RRAM *2013 5th IEEE Int. Mem. Work. IMW* 30–3
[15] Joshua Yang J, Miao F, Pickett M D, Ohlberg D A A, Stewart D R, Lau C N and Williams R S 2009 The mechanism of electroforming of metal oxide memristive switches *Nanotechnology* **20** 215201
[16] Sharma A A, Noman M, Abdelmoula M, Skowronski M and Bain J A 2014 Electronic instabilities leading to electroformation of binary metal oxide-based resistive switches *Adv. Funct. Mater.* **24** 5522–9
[17] Schmitt R, Spring J, Korobko R and Rupp J L M 2017 Design of oxygen vacancy configuration for memristive systems *ACS Nano* **11** 8881–91
[18] Lübben M, Cüppers F, Mohr J, von Witzleben M, Breuer U, Waser R, Neumann C and Valov I 2020 Design of defect-chemical properties and device performance in memristive systems *Sci. Adv.* **6** eaaz9079
[19] Wu X *et al* 2011 Chemical insight into origin of forming-free resistive random-access memory devices *Appl. Phys. Lett.* **99** 133504
[20] Skaja K, Andrä M, Rana V, Waser R, Dittmann R and Baeumer C 2018 Reduction of the forming voltage through tailored oxygen non-stoichiometry in tantalum oxide ReRAM devices *Sci. Rep.* **8** 1–7
[21] Sharath S U, Joseph M J, Vogel S, Hildebrandt E, Komissinskiy P, Kurian J, Schroeder T and Alff L 2016 Impact of oxygen stoichiometry on electroforming and multiple switching modes in $TiN/TaO_x/Pt$ based ReRAM *Appl. Phys. Lett.* **109** 1–6
[22] Li Y, Sanna S, Norrman K, Christensen D V, Pedersen C S, Lastra J M G, Traulsen M L, Esposito V and Pryds N 2019 Tuning the stoichiometry and electrical properties of tantalum oxide thin films *Appl. Surf. Sci.* **470** 1071–4
[23] Brumbach M T, Mickel P R, Lohn A J, Mirabal A J, Kalan M A, Stevens J E and Marinella M J 2014 Evaluating tantalum oxide stoichiometry and oxidation states for optimal memristor performance *J. Vac. Sci. Technol.* A **32** 051403
[24] Stevens J E, Lohn A J, Decker S A, Doyle B L, Mickel P R and Marinella M J 2014 Reactive sputtering of substoichiometric Ta_2O_x for resistive memory applications *J. Vac. Sci. Technol.* A **32** 021501
[25] Lohn A J, Stevens J E, Mickel P R and Marinella M J 2013 Optimizing TaO_x memristor performance and consistency within the reactive sputtering 'forbidden region' *Appl. Phys. Lett.* **103** 063502
[26] Jiang H and Stewart D A 2017 Using dopants to tune oxygen vacancy formation in transition metal oxide resistive memory *ACS Appl. Mater. Interfaces* **9** 16296–304
[27] Yildirim H and Pachter R 2019 Extrinsic dopant effects on oxygen vacancy formation energies in ZrO_2 with implication for memristive device performance *ACS Appl. Electron. Mater.* **1** 467–77
[28] Misha S H, Tamanna N, Woo J, Lee S, Song J, Park J, Lim S, Park J and Hwang H 2015 Effect of nitrogen doping on variability of TaO_x-RRAM for low-power 3-bit MLC applications *ECS Solid State Lett.* **4** P25–8
[29] Zhang H, Liu L, Gao B, Qiu Y, Liu X, Lu J, Han R, Kang J and Yu B 2011 Gd-doping effect on performance of HfO_2 based resistive switching memory devices using implantation approach *Appl. Phys. Lett.* **98** 1–4
[30] Yu S, Gao B, Dai H, Sun B, Liu L, Liu X, Han R, Kang J and Yu B 2010 Improved uniformity of resistive switching behaviors in HfO_2 thin films with embedded Al layers *Electrochem. Solid-State Lett.* **13** 36–9
[31] Kasatikov S, Filatova E, Sakhonenkov S, Konashuk A and Makarova A 2019 Relationship between Ta oxidation state and its local atomic coordination symmetry in a wide range of oxygen nonstoichiometry extent of TaO_x *J. Phys. Chem.* C **123** 6849–60
[32] Kröger F A and Vink H J 1956 Relations between the Concentrations of Imperfections in Crystalline Solids *Solid State Physics* (3) ed F Seitz and D Turnbull (New York: Academic) 307–435
[33] Tyuliev G and Angelov S 1988 The nature of excess oxygen in $Co_3O_{4+\epsilon}$ *Appl. Surf. Sci.* **32** 381–91

[34] Naeem M, Hasanain S K, Kobayashi M, Ishida Y, Fujimori A, Buzby S and Shah S I 2006 Effect of reducing atmosphere on the magnetism of $Zn_{1-x}Co_xO$ ($0 \leqslant x \leqslant 0.10$) nanoparticles *Nanotechnology* **17** 2675–80
[35] Park S M, Hwang H G, Woo J U, Lee W H, Chae S J and Nahm S 2020 Improvement of conductance modulation linearity in a Cu^{2+}-doped $KNbO_3$ memristor through the increase of the number of oxygen vacancies *ACS Appl. Mater. Interfaces* **12** 1069–77
[36] Kim S, Choi S, Lee J and Lu W D 2014 Tuning resistive switching characteristics of tantalum oxide memristors through Si doping *ACS Nano* **8** 10262–9
[37] Ismail M, Hashmi A, Rana A M and Kim S 2020 Eradicating negative-Set behavior of TiO_2-based devices by inserting an oxygen vacancy rich zirconium oxide layer for data storage applications *Nanotechnology* **31** 325201
[38] Sarma D D and Rao C N R 1980 XPES studies of oxides of second- and third-row transition metals including rare earths *J. Electron Spectrosc. Relat. Phenom.* **20** 25–45
[39] Liu J, Liao M, Imura M, Tanaka A, Iwai H and Koide Y 2014 Low on-resistance diamond field effect transistor with high-k ZrO_2 as dielectric *Sci Rep.* **4** 6395
[40] Jellison G E and Modine F A 1996 Parameterization of the optical functions of amorphous materials in the interband region *Appl. Phys. Lett.* **69** 371–3
[41] Ferlauto A S, Ferreira G M, Pearce J M, Wronski C R, Collins R W, Deng X and Ganguly G 2002 Analytical model for the optical functions of amorphous semiconductors from the near-infrared to ultraviolet: applications in thin film photovoltaics *J. Appl. Phys.* **92** 2424–36
[42] Demiryont H, Sites J R and Geib K 1985 Effects of oxygen content on the optical properties of tantalum oxide films deposited by ion-beam sputtering *Appl. Opt.* **24** 490
[43] Lee J, Lu W D and Kioupakis E 2017 Electronic and optical properties of oxygen vacancies in amorphous Ta_2O_5 from first principles *Nanoscale* **9** 1120–7
[44] Lee J, Schell W, Zhu X, Kioupakis E and Lu W D 2019 Charge transition of oxygen vacancies during resistive switching in oxide-based RRAM *ACS Appl. Mater. Interfaces* **11** 11579–86
[45] Gritsenko V A, Volodin V A, Perevalov T V, Kruchinin V N, Gerasimova A K, Aliev V S and Prosvirin I P 2018 Nanoscale potential fluctuations in nonstoichiometrics tantalum oxide *Nanotechnology* **29** 425202
[46] Graves C E, Dávila N, Merced-Grafals E J, Lam S T, Strachan J P and Williams R S 2017 Temperature and field-dependent transport measurements in continuously tunable tantalum oxide memristors expose the dominant state variable *Appl. Phys. Lett.* **110** 123501
[47] Zaima S 1990 Conduction mechanism of leakage current in Ta_2O_5 films on Si prepared by LPCVD *J. Electrochem. Soc.* **137** 2876
[48] Zhang Y, Deng N, Wu H, Yu Z, Zhang J and Qian H 2014 Metallic to hopping conduction transition in Ta_2O_{5-x}/TaO_y resistive switching device *Appl. Phys. Lett.* **105** 1–5
[49] Chiu F C 2014 A review on conduction mechanisms in dielectric films *Adv. Mater. Sci. Eng.* **2014** 578168
[50] Fang R, Chen W, Gao L, Yu W and Yu S 2015 Low-temperature characteristics of HfO_x based resistive random access memory *IEEE Electron Device Lett.* **36** 567–9
[51] Perevalov T V, Gritsenko V A, Gismatulin A A, Voronkovskii V A, Gerasimova A K, Aliev V S and Prosvirin I A 2018 Electronic structure and charge transport in nonstoichiometric tantalum oxide *Nanotechnology* **29** 264001
[52] Gritsenko V A, Perevalov T V, Voronkovskii V A, Gismatulin A A, Kruchinin V N, Aliev V S, Pustovarov V A, Prosvirin I P and Roizin Y 2018 Charge transport and the nature of traps in oxygen deficient tantalum oxide *ACS Appl. Mater. Interfaces* **10** 3769–75
[53] Goldfarb I and Williams R S 2014 Conduction centers in a $Ta_2O_{5-\delta}$ Fermi glass *Appl. Phys.* A **114** 287–9
[54] Goldfarb I, Miao F, Yang J J, Yi W, Strachan J P, Zhang M X, Pickett M D, Medeiros-Ribeiro G and Williams R S 2012 Electronic structure and transport measurements of amorphous transition-metal oxides: observation of fermi glass behavior *Appl. Phys.* A **107** 1–11
[55] Wei Z *et al* 2011 Demonstration of high-density ReRAM ensuring 10-year retention at 85 °C based on a newly developed reliability model *2011 International Electron Devices Meeting* pp 31.4.1–4
[56] Wang C, He W, Tong Y and Zhao R 2016 Investigation and manipulation of different analog behaviors of memristor as electronic synapse for neuromorphic applications *Sci. Rep.* **6** 1–9
[57] Prakash A, Deleruyelle D, Song J, Bocquet M and Hwang H 2015 Resistance controllability and variability improvement in a TaO_x-based resistive memory for multilevel storage application *Appl. Phys. Lett.* **106** 233104
[58] Ambrogio S, Member S, Balatti S, Member S, Cubeta A, Calderoni A, Ramaswamy N, Member S, Ielmini D and Member S 2014 Statistical fluctuations in HfO_x resistive-switching memory: I. Set/reset variability *IEEE Trans. Electron Devices* **61** 2912–9